coatings

MDPI

Article

Influence of TiO_2-Coating Layer on Nanoporous Alumina Membranes by ALD Technique

Lourdes Gelde [1], Ana L. Cuevas [2], María del Valle Martínez de Yuso [3], Juana Benavente [1,*], Víctor Vega [4], Ana Silvia González [5], Víctor M. Prida [5] and Blanca Hernando [5]

1 Department of Física Aplicada I, Facultad de Ciencias, Universidad de Málaga, E-29071 Málaga, Spain; geldelourdes@hotmail.com
2 Unidad de Nanotecnología, SCBI Centro, Universidad de Málaga, E-29071 Málaga, Spain; analaura.cuevas@uma.es
3 Servicios Centrales de Investigación, Universidad de Málaga, E-29071 Málaga, Spain; mvyuso@uma.es
4 Laboratorio de Membranas Nanoporosas, Servicios Científico-Técnicos, Universidad de Oviedo, E-33006 Oviedo, Spain; vegavictor@uniovi.es
5 Department of Física, Facultad de Ciencias, Universidad de Oviedo, E-33007 Oviedo, Spain; gonzalezgana@uniovi.es (A.S.G.); vmpp@uniovi.es (V.M.P.); grande@uniovi.es (B.H.)
* Correspondence: j_benavente@uma.es; Tel.: +34-952-131-929

Received: 15 December 2017; Accepted: 31 January 2018; Published: 7 February 2018

Abstract: Geometrical, chemical, optical and ionic transport changes associated with ALD of TiO_2-coating on the porous structure of two nanoporous alumina membranes (NPAMs), which were obtained by the two-step aluminum anodization method but with different pore size and porosity, are presented. Chemical and morphological changes were determined by analyzing XPS spectra and SEM images, showing practically total coverage of the NPAMs surface and leading to a reduction in the geometrical parameters of both samples, while SAED and high resolution TEM measurements allowed us to determine the crystalline structure and thickness of the TiO_2-coating, with the latter confirmed by depth-profile XPS analysis. Spectroscopic ellipsometry measurements were also carried out in order to detect changes in characteristic optical parameters (refractive index, n, and extinction coefficient, k), due to the TiO_2-coating of NPAMs. Considering the common application of NPAMs in solute/ion diffusion processes, the effect of the TiO_2-coverage on electrochemical parameters was analyzed by measuring the concentration potential with a typical model electrolyte (KCl solutions), leading to an increase of the electropositive character for both kinds of samples.

Keywords: nanoporous alumina membranes; ALD; TiO_2-coating layer; SEM; TEM; XPS

1. Introduction

Nanoporous alumina membranes (NPAMs) that were obtained through the two-step aluminum anodization method, are systems of great interest due to their well-defined morphology (parallel cylindrical straight nano-pores with radius between 10 and 100 nm, inter-pore distances of 65–500 nm and narrow pore size distribution [1]), with applications in nanofiltration, biosensors or drug delivery [2–4]. Pore size and inter-pore distance/porosity of NPAMs depend on the anodization conditions, such as the value of the applied voltage, together with the electrolyte solution temperature and its pH used for the first anodization step, while pore length is mainly controlled by time associated with the second step of the anodization process [5]. However, changes induced in pore-size/porosity to get the most adequate morphological values for particular applications are also possible through a chemical pore-coating process, although these processes might also affect other NPAMs characteristics (selectivity, hydrophilic/hydrophobic character, electrochemical and optical properties) [6].

Atomic layer deposition (ALD) is a well-known thin film deposition technique that allows the surface modification by forming a homogeneous thin coating layer of different metal oxides with an accurate control of the thickness and composition at atomic scale [7]. The ALD technique is based on the vapor phase deposition method considering sequential and self-limiting reactions, which offers exceptional deposition conformality with high aspect ratio (quotient length to diameter) even for nanoporous structures. In particular, TiO_2 deposition into NPAMs by ALD technique has recently attracted broad scientific interest for their applications in biomedicine and photocatalysis [8–13].

Changes in different parameters associated with surface coating with a single layer of TiO_2 deposited by ALD technique on two NPAMs, with different pore size and porosity, are compared and discussed in this work. Chemical surface and structural modifications of the nanoporous alumina membranes were analyzed by X-ray photoelectron spectroscopy (XPS) spectra and scanning and transmission electron microscopy techniques (SEM and TEM, respectively). These analyses suggest the practically total coverage of the alumina supports with a uniform, polycrystalline anatase TiO_2 layer (Ti atomic concentrations of ~22% and around 1% for Al), leading to a pore size reduction of ~20%. Moreover, XPS depth-profile analysis was performed in order to check the chemical surface modification associated with the TiO_2-coating layer, whereas the spectroscopic ellipsometry technique has been used to determine the optical characteristics of both NPAMs and their modification due to the TiO_2-coating. Changes in ions diffusive transport associated with the pore-coatings were determined by concentration potential measurements performed with KCl solutions, which allows the determination of different electrochemical parameters (effective fixed charge concentration, ion transport numbers, ionic diffusion coefficients ratio) for the TiO_2-coated NPAMs, of great interest in nanofluidics, nanofiltration or drug-delivery applications. The set of samples studied and characterization techniques employed give us information on the effect of pore-radii, porosity and surface material (Al_2O_3 or TiO_2) on diffusive transport characteristics [14].

2. Materials and Methods

High purity aluminum discs (Al 99.999%, Goodfellow, Huntingdon, UK) with thickness of 0.5 mm and diameter of 25 mm were employed as starting substrates for the fabrication of the NPAMs by the well-established two-step electrochemical anodization approach. A 0.3 M solution of sulphuric acid at a constant anodization voltage of 25 V (Sf-NPAM membrane), or a 0.3 M solution of oxalic acid under an applied anodization voltage of 40 V (Ox-NPAM membrane), were respectively used for the first (and second) anodization processes, as it was extensively explained in ref. [15]. The duration of the first anodization step was fixed to 24 h in all the cases, in order to assure a high periodicity of nanopores self-ordering degree of NPAMs. The samples were then rinsed with deionized water. An aqueous solution of 0.2 M CrO_3 and 0.6 M H_3PO_4 was used for the selective removal of the anodic aluminum oxide layer grown in the first anodization step. To ensure the NPAMs integrity during fluid transport and optical measurements, an alumina membrane thickness of ~60 μm was selected, which was adjusted by controlling the duration of the second anodization step, performed under the same anodization conditions as in the first one. Other reagents such as isopropanol, ethanol, perchloric and orthophoshporic acids were used for aluminum cleaning, electropolishing and selective removal of the anodic aluminum oxide barrier layer.

ALD coating with TiO_2 thin layer of both NPAMs was performed in a Savannah 100 thermal ALD reactor from Cambridge Nanotech (Waltham, MA, USA). H_2O (at 60 °C) and titanium (IV) tetraisopropoxide (at 75 °C) were used as precursors for the conformal layer deposition, employing high purity Ar as the carrier gas. The NPAMs, heated at 200 °C in the reactor chamber, were sequentially exposed to the precursors which were injected into the reactor chamber employing pulsing times of 1 s. In order to allow the gaseous precursors for diffusing through the high aspect ratio pores of both NPAMs, the precursors were kept into the reaction chamber by closing the vacuum pump valve, during exposure times in the range of 45–60 s. To evacuate the excess of unreacted gaseous precursor and reaction by-products from the ALD reaction chamber, a purge during 90 s with Ar flow of 50 sccm

was performed between two subsequent precursor pulses. The number of coating cycles was adjusted according to a growth rate of 0.05 nm/cycle [16], in order to adjust the thickness of the TiO_2-coating layer to around 5 nm.

2.1. Chemical Surface Analysis

The chemical surface characterization of the as synthesized nanoporous alumina membranes and after being covered by ALD with a TiO_2-coating layer, was performed by XPS by using a Physical Electronics Spectrometer (PHI 5700, Physical Electronics, Chanhassen, MN, USA) with X-ray Mg Kα radiation (300W, 15 kV, 1253.6 eV) as the excitation source. High-resolution spectra were recorded at a take-off angle of 45° by a concentric hemispherical analyser operating in the constant pass energy mode at 29.35 eV, being the diameter of the analyzed area of 720 µm, and each spectral region was scanned several times until a good signal to noise ratio was observed. Binding energies (accurate $\pm$0.1 eV) were determined with respect to the position of the adventitious C 1*s* peak at 285.0 eV, maintaining the residual pressure in the analysis chamber below 5×10^{-7} Pa during data acquisition. PHI ACCESS ESCA-V6.0 F software package was used for data acquisition and analysis. Shirley-type background was subtracted from the signals, and the recorded spectra were fitted using Gauss-Lorentz curves for a more precise binding energy (BE) determination of the different element core levels [17]. Atomic concentration percentages (A.C. %) of the characteristic elements found on the membranes surfaces were determined taking into account the corresponding area sensitivity factor for the measured spectral regions [17].

XPS depth-profile analysis for the TiO_2-coated samples was also performed by argon sputtering (4 kV and 1.5 mA) during 8 minutes, which permits us an estimation of interfacial TiO_2/Al_2O_3 modifications and TiO_2-coverage on the pore-walls.

2.2. Scanning and Transmission Electron Microscopy Characterizations

Changes in the morphological parameters of NPAMs as a result of the ALD TiO_2-coating, as well as the nanopore channels in the cross section of mechanically broken samples, were studied by SEM analysis. Measurements were performed in a JEOL JSM-5600 microscope (Akishima, Tokyo, Japan), equipped with an Oxford INCA EDS microanalysis system (Oxford Instruments, Abingdon, UK). The SEM is fitted with a tungsten filament electron gun operating at an acceleration voltage of 20 kV. SEM images were obtained after coating the alumina membranes with a thin Au layer by magnetron sputtering deposition (Polaron SC7620, Quorum Technologies, Laughton, UK) at 20 mA for 180 s, to ensure their electrical conductivity, and they were further analysed by using ImageJ software (v 1.50i) [18].

The morphology and crystalline structure of the TiO_2 ALD coated samples were further studied by Transmission Electron Microscopy (TEM) and Selected Area Electron Diffraction (SAED) performed in a JEOL JEM 2100 (Akishima, Tokyo, Japan), a 200 kV analytical electron microscope that is suited with an advanced field emission electron gun. The TiO_2-coated NPAMs were selectively etched in CrO_3 and H_3PO_4 aqueous solution in order to dissolve the alumina matrix, thus leaving freestanding TiO_2 nanotubes. The samples were then filtered and suspended in ethanol and deposited dropwise in a carbon coated copper TEM grid.

2.3. Spectroscopic Ellipsometry Measurements

For optical characterization, spectroscopic ellipsometry measurements were performed with a commercial spectroscopic ellipsometer (GES 5E, Semilab, Budapest, Hungary), with a wavelength covering visible and near-ultraviolet regions (between 1.0 and 5.5 eV), at a fixed incidence angle of 65°. Winelli software (v 2.2.0.7, Semilab, Budapest, Hungary) was used for real and imaginary parts of the complex refraction index determination from experimental parameters.

2.4. Concentration Potential Measurements

Concentration potential, or the equilibrium electrical potential difference between two electrolyte solutions of different concentration (C_f and C_v) separated by a membrane or permselective structure, was measured in a dead-end test cell consisting of two glass half-cells, with a magnetic stirrer in the bottom of each half-cell to minimize the concentration-polarization at the membrane (nanoporous structure)/solution interfaces (stirring rate of 540 rpm) [19]. Two Ag/AgCl reversible electrodes, one placed at each half-cell, were connected to a digital voltmeter (Yokohama 7552, 1GΩ input resistance) for cell potential (ΔE) measurements, which were performed with different KCl solutions (at 25 ± 2 °C, pH = 5.9 ± 0.2) by keeping constant the concentration of the solution at one side of the membrane (C_f = 0.01 M) and gradually changing the concentration of the solution at the other side (0.002 M ≤ C_v ≤ 0.1 M). Membrane potential values ($\Delta\Phi_{mbr}$) were obtained for each pair of (C_v, C_f) concentrations by subtracting the electrode potential ($\Delta\Phi_{elect} = (RT/F) \times \ln(C_v/C_f)$) to the corresponding cell potential value, that is, $\Delta\Phi_{mbr} = \Delta E - \Delta\Phi_{elect}$.

3. Results

3.1. Chemical and Morphological Characterization of the Nanoporous Alumina-Based Membranes

Figure 1 shows top-view SEM micrographs of the surface of both, the Ox- and Sf-NPAMs (Figure 1a,d, respectively), as well as the corresponding samples coated with TiO_2 by ALD (Ox-NPAM + TiO_2 (Figure 1b) and Sf-NPAM + TiO_2 (Figure 1e)) The highly ordered and close-packed hexagonal nanoporous structure characteristic of this kind of alumina-based sample is clearly evident. From these pictures, the average values of pore radius, r_p, and inter-pore distance, D_{int}, were obtained using the Image J software. Table 1 collects these values, as well as those values obtained for the membranes porosity, Θ, determined through the relationship: $\Theta = (2\pi/\sqrt{3})(r_p/D_{int})^2$ [20]. A noticeable reduction in both, pore diameter and porosity associated with the conformally ALD deposited TiO_2-layer can be observed for both Ox-NPAM + TiO_2 and Sf-NPAM + TiO_2 samples. SEM cross section images of the Ox- and Sf-NPAM, shown in Figure 1c,f respectively, evidence the existence of straight pore channels, parallel aligned to each other.

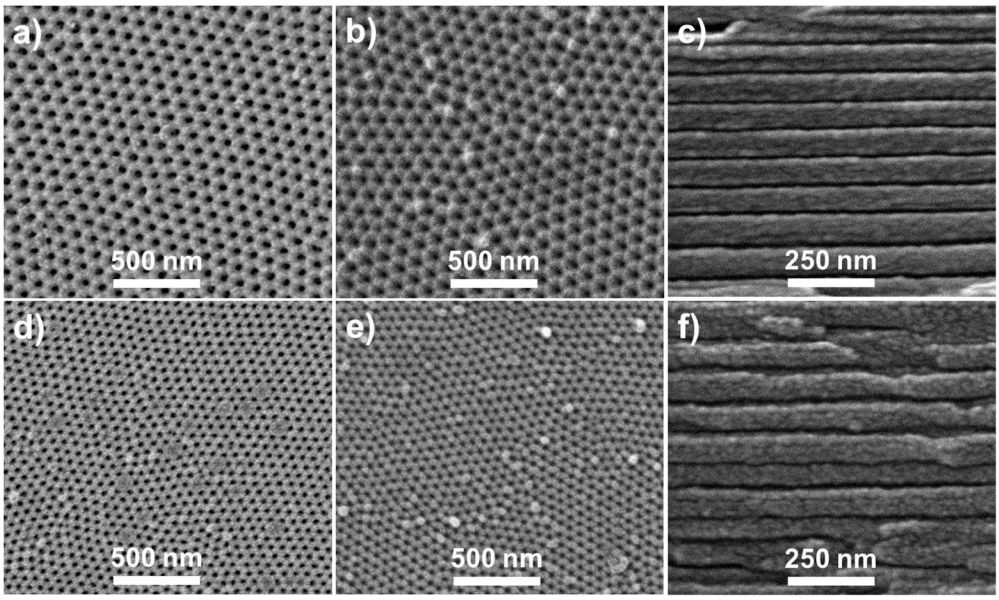

Figure 1. SEM micrographs at the surface of: (**a**) Ox-NPAM; (**b**) Ox-NPAM + TiO_2; (**d**) Sf-NPAM and (**e**) Sf + NPAM + TiO_2 samples. Images (**c**,**f**) show a cross section view of the channels of Ox- and Sf-NPAMs, respectively.

Table 1. Morphological parameters characteristic of the studied membrane: pore radii (r_p), inter-pore distance (D_{int}), and estimated average porosity (Θ), calculated according to ref. [20].

Membrane	r_p (nm)	D_{int} (nm)	Θ (%)
Ox-NPAM	16 ± 2	105 ± 5	8
Ox-NPAM + TiO_2	13 ± 2	105 ± 5	6
Sf-NPAM	13 ± 2	65 ± 5	13
Sf-NPAM + TiO_2	10 ± 2	65 ± 5	9

TEM characterization of the TiO_2-coating on Ox-NPAM + TiO_2 is shown in Figure 2, indicating that the ALD deposits exhibit a nanocrystalline structure, which can be indexed to anatase phase of titanium dioxide [21], similar to that reported in the literature for ALD deposited TiO_2 films. Despite the lower deposition temperature employed in our work [8,10] and the fact that our samples were not annealed after deposition [11,12], our results are in good agreement with those obtained for the same precursors and deposition temperature [16]. The thickness of the ALD deposit can be estimated from TEM images by the measurement of TiO_2 nanotube wall thickness as shown in Figure 2a [12], and it takes values around 5 nm in good agreement with manufacture condition previously indicated.

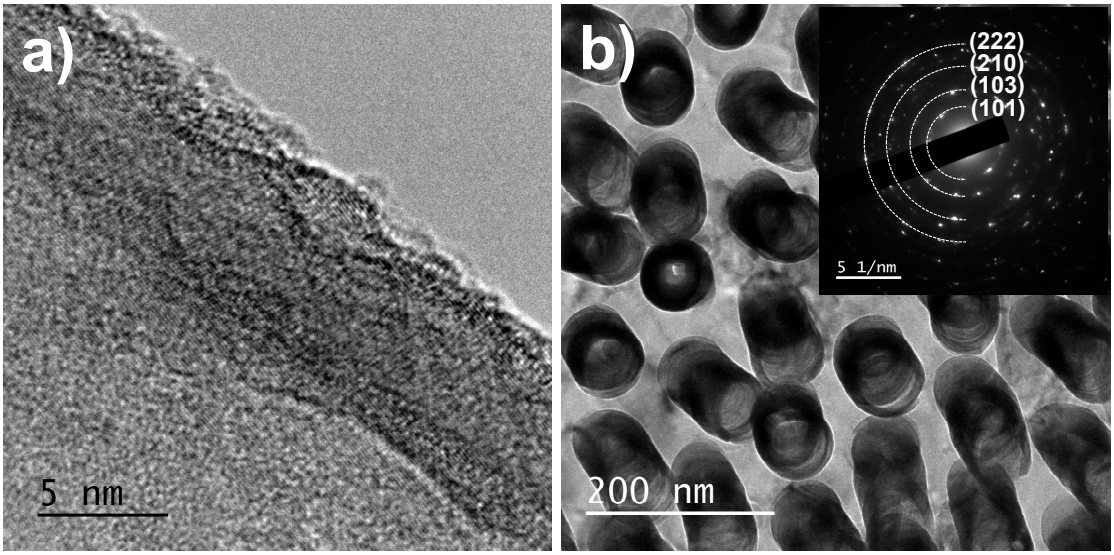

Figure 2. TEM images of TiO_2-coating deposited by ALD. (**a**) High magnification image of TiO_2 nanotubes; (**b**) Top-view of the TiO_2 nanotube arrays. The inset in (**b**) shows SAED spectrum of nanotubes, indexed to the anatase phase of TiO_2.

The surface chemistry of the nanoporous structures was analyzed by XPS spectra, and a comparison of the core level signals obtained for the different elements found are shown in Figure 3. The aluminum Al 2*p* core level signal in Figure 3a shows similar and well-defined peaks for both NPAM samples, but its contribution is practically undetectable in the case of the TiO_2-covered NPAM, while no differences can be observed in the Ti 2*p* doublet (Figure 3b) obtained for these latter samples. Figure 3c shows the O 1*s* core level signal for the Ox-NPAM, which shows a peak with a maximum at around 531.8 eV due to alumina, plus a small contribution at lower B.E. (530.5 eV) associated with carboxylate groups. The Ox-NPAM + TiO_2 spectra presents a clear peak at 529.5 eV, which corresponds to titania, and a small shoulder at around 531.8 eV due to the alumina oxygen [17]. Moreover, Figure 3d shows the C 1*s* core level signal, where a clear peak at 285.0 eV (C–C and aliphatic carbon) can be observed, as well as another small peak at 288.5 eV (O–C=O link) and a shoulder at 286.0 eV (C–O–C bond) [17]. The presence of carbon in the analyzed samples is associated with manufacture and ALD processes, in addition to environmental contamination [22].

The atomic concentration percentages of the different elements present at the nanoporous structures surfaces were obtained from the peak areas for each element, whose obtained values are indicated in Table 2. These results demonstrate the near total coverage of both NPAMs by the ALD coated TiO_2-layer, as well as a significantly high percentage of carbon surface contamination. Moreover, incorporation of carbon containing ions in the samples obtained by anodization in oxalic acid electrolytes [5] seems to exist, according to the higher carbon A.C. % detected for such samples.

Depth-profile analysis for the TiO_2-coated NPAMs was also performed for analyzing the chemical changes associated with the TiO_2-coverage. Figure 4 shows the variation of the titanium, aluminium, oxygen and carbon atomic concentrations as a function of the sputtering time for the Ox-NPAM + TiO_2 sample. From these results, and taking into account the different sputtering-time factors for pure materials, a thickness of around 6 nm was estimated for the deposited TiO_2 superficial layer. They also show the very superficial character of the environmental carbon contribution (<3 nm) associated with atmospheric contamination and the increase in titanium (16%) and oxygen (12%) percentages with environmental carbon contamination reduction during approximately the first minute of the sputtering process. Moreover, the presence of TiO_2-coating along the pore-walls can also be inferred from these results, according to the constancy of titanium atomic concentration with the sputtering time (or depth-profile) as it is schematically indicated in the insert of the Figure 4, in agreement with those previously obtained by using local energy dispersive X-ray spectroscopy (EDS) analysis [23].

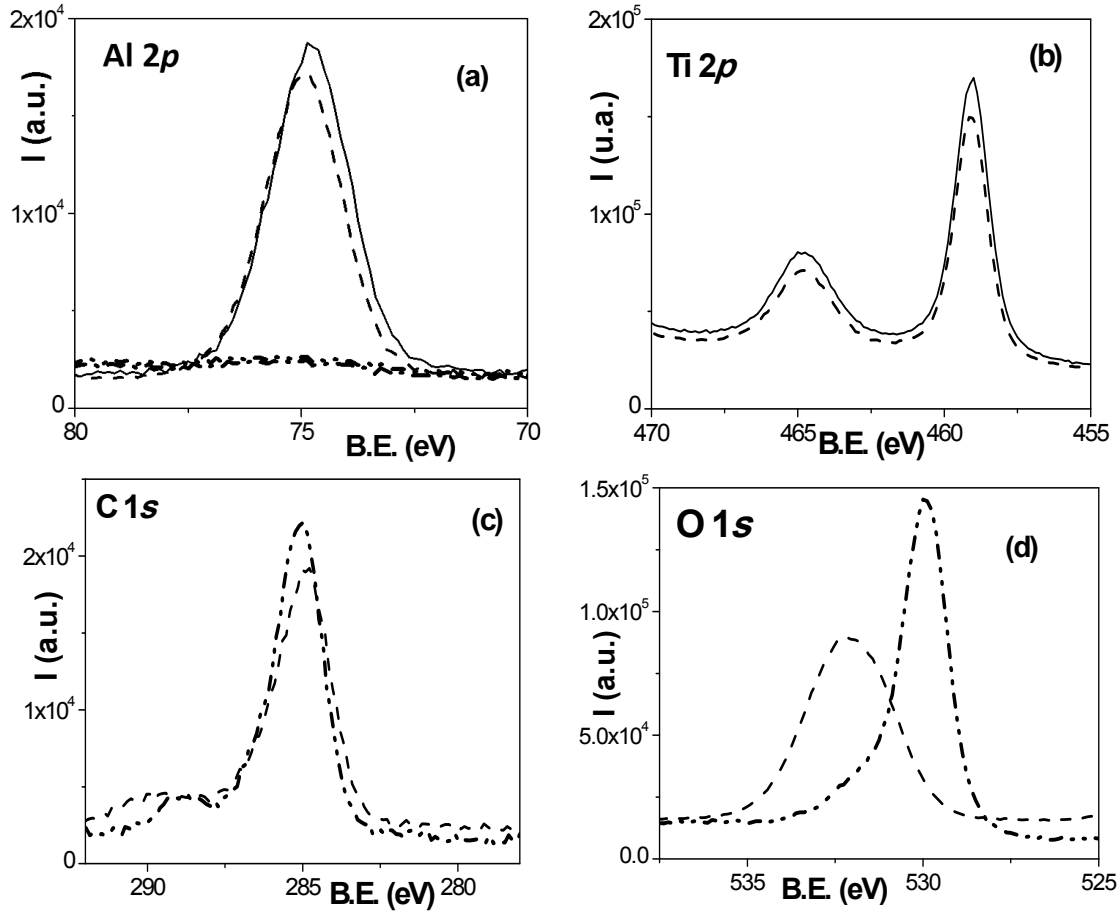

Figure 3. (**a**) Al 2*p* core level spectra for Sf-NPAM (solid), Ox-NPAM (dash), Sf-NPAM + TiO_2 (dotted dotted), Ox-NPAM + TiO_2 (dotted dash); (**b**) Ti 2*p* core level spectra for Sf-NPAM + TiO_2 (solid), Ox-NPAM + TiO_2 (dash). Comparison of core level spectra for Ox-NPAM (dotted) and Ox-NPAM + TiO_2 (dotted dash): (**c**) C 1*s* and (**d**) O 1*s*.

Table 2. Atomic concentration percentages of the elements found on both surfaces of the studied samples *.

Sample	C (%)	Al (%)	Ti (%)	O (%)	N (%)	Si (%)
Sf-NPAM [a]	16.9	25.7	–	53.0	–	0.3
Sf-NPAM + TiO_2	19.2	0.6	23.5	53.5	0.7	0.5
Ox-NPAM [b]	23.8	25.3	–	48.3	–	0.3
Ox-NPAM + TiO_2	24.4	1.5	21.4	52.2	0.2	0.4

* Other elements with A.C. % < 0.3 are not indicated. [a] Plus 2.2% of sulphur and 1.9% of phosphorus; [b] Plus 2.3% of sulphur.

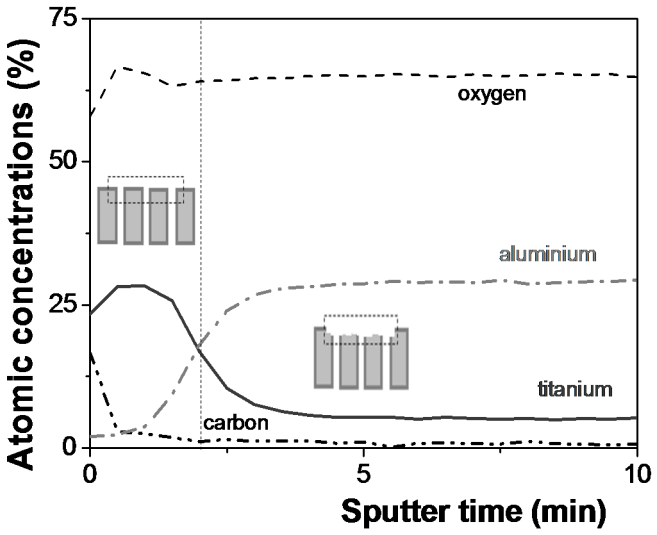

Figure 4. Ox-NPAM + TiO_2 sample sputtering time dependence (profile curves) of titanium, aluminum, oxygen and carbon atomic concentrations. The insets schematize the effect of the argon sputtering on the TiO_2-coated nanoporous structure.

3.2. Spectroscopic Ellipsometry Analysis

Application of spectroscopic ellipsometry to the study of optical properties of nanoporous alumina structures obtained by electrochemical aluminum anodization has already been performed by different authors [24,25], and differences depending on the pore radii/porosity of the studied samples have been reported [26]. Ellipsometry measures a change in the polarization as light reflects or transmits from a material structure, and the ellipsometric angles Ψ and Δ, determine the differential changes in amplitude and phase, respectively ($\tan(\Psi)\, e^{i\Delta} = r_p/r_s$, where r_p y r_s are the amount of light reflected in the perpendicular and parallel planes of incidence [27]). Consequently, spectroscopic ellipsometry measurements of the TiO_2-coated NPAMs might also provide information on the optical changes associated with the coated layer; in particular, information on the real part of the complex refractive index (n) and the imaginary part of the complex refractive index or extinction coefficient (k), can be respectively obtained from these measurements. Figure 5 shows a comparison of wavelength dependence of measured Ψ and Δ parameters (tan(Ψ) in Figure 5a and cos(Δ) in Figure 5b) for Ox-NPAM and Ox-NPAM + TiO_2 samples. Differences associated with TiO_2-coating can be observed in Figure 5, which seem to be related to pore radius modification, in agreement with the SEM results; similar curves were also obtained for the Sf-NPAM and Sf-NPAM + TiO_2 samples.

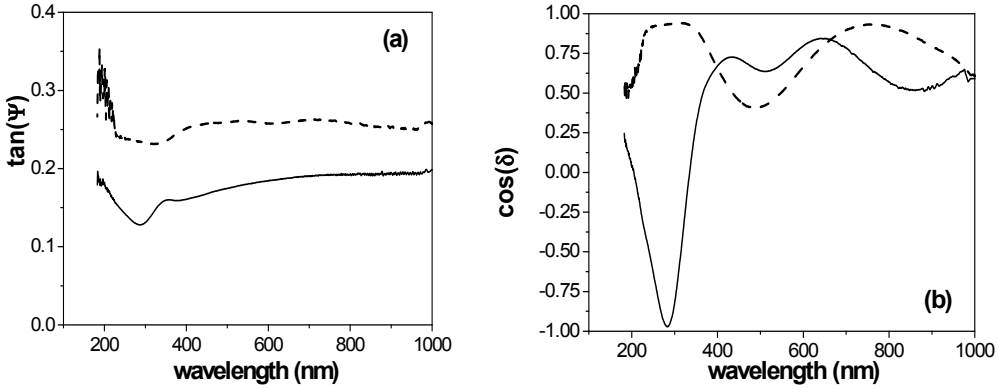

Figure 5. Wavelength dependence for changes in the light phase angle (**a**) and amplitude (**b**) for the Ox-NPAM (dashed line) and the Ox-NPAM + TiO_2 (solid line).

From this measurement, using the ellipsometer software and assuming a homogeneous dense substrate in contact with air, the real (n) and imaginary (k) parts of the complex refractive index were determined and their dependence with the wavelength is shown in Figure 6 for both, the Ox-NPAM and Ox-NPAM + TiO_2 samples. A rather constant value for the reflexive index n, in the range between 400 and 1000 nm, can be observed, but also its increase in around 10% for the TiO_2-covered sample. For comparison, the values obtained at λ = 632.8 nm [26] for the different nanoporous structures are indicated in Table 3. As expected, n values for the NPAMs are slightly lower than that given in the literature for "solid" alumina at that particular λ value ($n Al_2O_3$ = 1.774), which is mainly due to the porous character of the studied samples (consequently, a "mixture" of alumina and air), but the effect of material impurities should also be considered. This fact, as well as the composite character and possible higher surface nano-rugosity of the coated samples, which significantly influence the ellipsometry measurements, can explain the difference in n and k values obtained for the NPAM + TiO_2 samples, when compared with pure TiO_2 films or nanoparticles at the given wavelength.

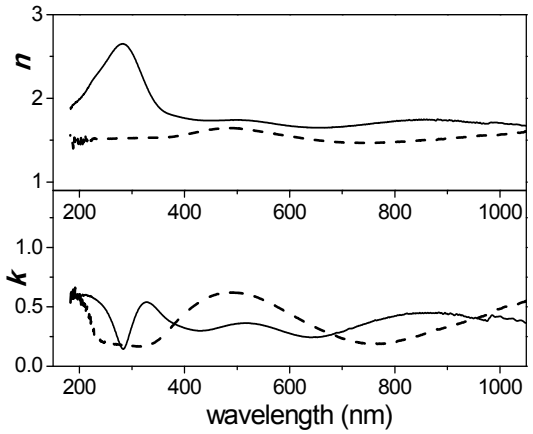

Figure 6. Wavelength dependence of the refraction index, n, and the extinction coefficient, k, for the Ox-NPAM (dashed line) and the Ox-NPAM + TiO_2 (solid line).

Table 3. Refractive index (n) and extinction coefficient (k) at a wavelength of 632.8 nm.

Sample	*n*	*k*
Sf-NPAM	1.6091	0.4909
Sf-NPAM + TiO_2	1.4606	0.3359
Ox-NPAM	1.5151	0.3657
Ox-NPAM + TiO_2	1.6527	0.2458

3.3. Concentration Potential Analysis

As it is well known, transport of solutions across nanoporous membranes (or nanostructures) is a research field of significant importance with technological applications in microfluidics, drug delivery or nanofilters [28,29]. Diffusive transport of saline solutions across membranes is usually characterized by the effective fixed charge concentration in the membrane (X_{ef}) and the ionic transport numbers (t_i), which represents the fraction of the total current flowing through the membrane transported for one ion ($t_i = I_i/I_T$), or the diffusion coefficients (D_i) related to t_i through the following electrochemical relationship: $D_i = t_i/(t_+ + t_-)$, for 1:1 electrolytes [30]. Membrane (or solid structure) equivalent fixed charge might avoid/reduce the transport of co-ions (ions of equal sign as the charged solid surface) and favor the diffusive transport of counter-ions, which usually affects the transport number of ions or charged species across porous structures and, consequently, modifies the diffusion potential in the membrane [31]. Moreover, the charged membrane/solid matrix also affects the ions distribution at both solution/solid interfaces, associated with Donnan equilibrium (Donnan potential). According to the Teorell–Meyer–Sievers (TMS) model [32,33], the equilibrium electrical potential difference between the two electrolyte solutions of concentrations (C_f and C_v) separated by a membrane or membrane potential can be expressed by [34]:

$$\Delta\Phi_{mbr} = -\frac{RT}{wzF}\left[U \ln \frac{\sqrt{4y_v^2+1}+wU}{\sqrt{4y_f^2+1}+wU} - \ln \frac{cf}{cv}\frac{\sqrt{4y_v^2+1}+w}{\sqrt{4y_f^2+1}+w}\right] \quad (1)$$

where F and R represent the Faraday and gas constants, T indicates the temperature of the system and $w = (+1)$ or (-1) depending on the electrical character (positive or negative fixed charge) of the membrane. The parameter U is related to the ion transport numbers and $y_i = C_i/|X_f|$ (partition coefficient at the membrane/solution concentration can be taken as (1). Figure 7 shows a comparison of the membrane potential for the studied samples, where differences associated with both pore size and surface material can be observed; for comparison, membrane potentials for an ideal anion-exchanger, that is, a positively charged system with $t_- = 1$ and $t_+ = 0$, are also indicated in Figure 7 by the dense straight-line. In particular, according to the similarity of the values indicated in Figure 7 for the Sf-NPAM + TiO_2 and the ideal anion-exchanger, low cation transport across this sample is expected for the whole range of KCl concentration.

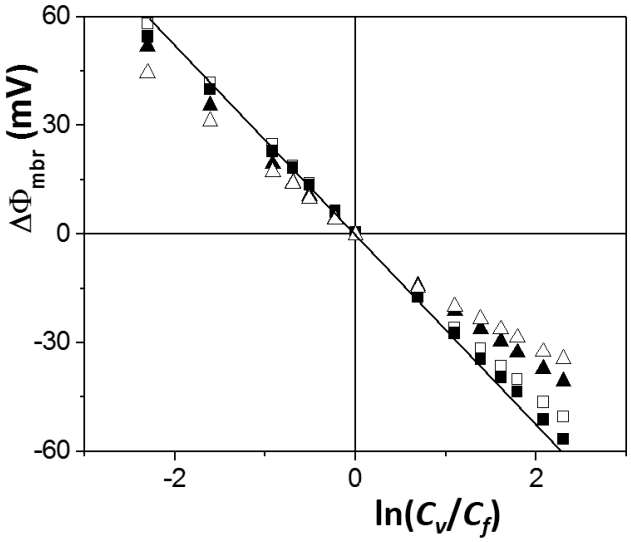

Figure 7. Membrane potential as a function of the solutions concentration ratio for: (□) Sf-NPAM, (■) Ox-NPAM, (Δ) Sf-NPAM + TiO_2 and (▲) Ox-NPAM + TiO_2.

The fitting to Equation (1) of the values shown in Figure 7, by following the calculation procedure indicated in previous papers [17,29], allows for the determination of the ion transport numbers across the nanoporous structures (t_i) as well as the ionic diffusion coefficient ratios ($D_-/D_+ = t_-/t_+$), and their values are indicated in Table 4, where differences associated with both pore size and material surface on diffusive ionic transport can be observed. An increase in ionic effect with pore size reduction was expected and already demonstrate for neutral molecules [13], but the significant contribution of electrical interactions in this kind of system [35,36] could also affect the transport of charged species. Moreover, these results also show the effect of the TiO_2-coating on the anionic selective character of the NPAMs, independently of the pore radii.

Table 4. Cation transport number (t_{K^+}) and ionic diffusion coefficients ratio (D_{Cl^-}/D_{K^+}) for the studied NPAMs and NPAMs+TiO_2 samples.

Sample	t_{K^+}	D_{Cl^-}/D_{K^+}
Sf-NPAM	0.292	2.43
Sf-NPAM + TiO_2	0.162	5.17
Ox-NPAM	0.310	2.23
Ox-NPAM + TiO_2	0.187	4.35

4. Discussion

Modification of two NPAMs by a coating layer of TiO_2 of 5–6 nm of thickness on the surface and along the nanopores, according to TEM images and XPS depth-profile analysis, has permitted us to analyze different effects (pore size and porosity reduction as well as surface material) on characteristic optical parameters and diffusive transport of an electrolyte solution. In fact, spectroscopic ellipsometry measurements show differences in refractive index and extinction coefficient depending on both pore-radii/porosity and material. However, different factors (composite structure for the NPAM + TiO_2 samples, manufacture impurities, surface nano-roughness) do not allow a direct correlation with pure material values, although the lower values for the extinction coefficient of NPAM + TiO_2 samples agrees with the almost transparent character of titania at the selected wavelength. On the other hand, with respect to the diffusive transport, it is interesting to note the lower cation transport number and higher D_-/D_+ ratio exhibited by the Ox-NPAM + TiO_2 sample when compared with the Sf-NPAM one, both with similar pore radii (13 nm) but different surface material, which is an indication of higher selectivity of TiO_2 to K^+ ions than Al_2O_3. As expected for membranes with similar surface material, the increase in pore size reduces ionic selectivity. Consequently, TiO_2-coating of NPAMs by the ALD technique seems to be an adequate method for geometrical and functional changes of alumina-based nanoporous membranes (or structures), opening their field of application.

Acknowledgments: This work has been financially supported under Spanish MINECO research Project No. MAT2016-76824-C3-3-R and Principality of Asturias (FICyT) Project No. FC-15-GRUPIN14-085. The scientific support of the Laboratory of Nanoporous Membranes and facilities from SCTs of University of Oviedo are also recognized.

Author Contributions: Juana Benavente, Víctor M. Prida and Blanca Hernando conceived and designed the experiments. Ana Silvia González and Víctor Vega synthesized the ALD-coated membranes and performed electron microscopy analysis of the samples. Membrane potential measurements, data interpretation and analysis were performed by Lourdes Gelde and Juana Benavente, María del Valle Martínez de Yuso is responsible of XPS measurements and Ana L. Cuevas has carried out spectroscopic ellipsometry measurements. All authors have contributed in co-writing of the manuscript and gave approval to the final revision.

Conflicts of Interest: The authors declare no conflict of interest.

References

1. Masuda, H.; Fukuda, K. Ordered metal nanohole arrays made by a two-step replication of honeycomb structures of anodic alumina. *Science* **1995**, *268*, 1466–1468. [CrossRef] [PubMed]

2. Hohlbein, J.; Steinhart, M.; Schiene-Fisher, C.; Benda, A.; Hof, M.; Hübner, C.G. Confined Diffusion in Ordered Nanoporous Alumina Membranes. *Small* **2007**, *3*, 380–385. [CrossRef] [PubMed]
3. Jiang, X.; Mishra, N.; Turner, J.N.; Spencer, M.G. Diffusivity of sub-1000 Da molecules in 40 nm silicon-based alumina pores. *Microfluid. Nanofluid.* **2008**, *5*, 695–701. [CrossRef]
4. Karnik, R.; Fan, R.; Yue, M.; Li, D.; Yang, P.; Majumdar, A. Electrostatic Control of Ions and Molecules in Nanofluidic Transistors. *Nano Lett.* **2005**, *5*, 943–948. [CrossRef] [PubMed]
5. Lee, W.; Park, S.J. Porous Anodic Aluminum Oxide: Anodization and Templated Synthesis of Functional Nanostructures. *Chem. Rev.* **2014**, *114*, 7487–7556. [CrossRef] [PubMed]
6. Romero, V.; Vega, V.; García, J.; Zierold, R.; Nielsch, K.; Prida, V.M.; Hernando, B.; Benavente, J. Changes in Morphology and Ionic Transport Induced by ALD SiO_2 Coating of Nanoporous Alumina Membranes. *ACS Appl. Mater. Interfaces* **2013**, *5*, 3556–3564. [CrossRef] [PubMed]
7. George, S.M. Atomic Layer Deposition: An Overview. *Chem. Rev.* **2010**, *110*, 111–131. [CrossRef] [PubMed]
8. Narayan, R.J.; Monteiro-Riviere, N.A.; Brigmon, R.L.; Pellin, M.J.; Elam, J.W. Atomic Layer Deposition of TiO_2 Thin Films on Nanoporous Alumina Templates: Medical Applications. *JOM* **2009**, *61*, 12–16. [CrossRef]
9. Petrochenko, P.E.; Kumar, G.; Fu, W.; Zhang, Q.; Zheng, J.; Liang, C.; Goering, P.L.; Narayan, R.J. Nanoporous Aluminum Oxide Membranes Coated with Atomic Layer Deposition-Grown Titanium Dioxide for Biomedical Applications: An In Vitro Evaluation. *J. Biomed. Nanotechnol.* **2015**, *11*, 2275–2285. [CrossRef] [PubMed]
10. Kemell, M.; Pore, V.; Tupala, J.; Ritala, M.; Leskelä, M. Atomic Layer Deposition of Nanostructured TiO_2 Photocatalysts via Template Approach. *Chem. Mater.* **2007**, *19*, 1816–1820. [CrossRef]
11. Ng, C.J.W.; Gao, H.; Tan, T.T.Y. Atomic Layer Deposition of TiO_2 nanostructures for self-cleaning applications. *Nanotechnology* **2008**, *19*. [CrossRef] [PubMed]
12. Liang, Y.-C.; Wang, C.-C.; Kei, C.-C.; Hsueh, Y.-C.; Cho, W.-H.; Perng, T.-P. Photocatalysis of Ag-Loaded TiO_2 Nanotube Arrays Formed by Atomic Layer Deposition. *J. Phys. Chem. C* **2011**, *115*, 9498–9502. [CrossRef]
13. Cameron, M.A.; Gartland, I.P.; Smith, J.A.; Diaz, S.F.; George, S.M. Atomic Layer Deposition of SiO_2 and TiO_2 in Alumina Tubular Membranes: Pore Reduction and Effect of Surface Species on Gas Transport. *Langmuir* **2000**, *16*, 7435–7444. [CrossRef]
14. Romero, V.; Vega, V.; García, J.; Prida, V.M.; Hernando, B.; Benavente, J. Ionic transport across tailored nanoporous anodic alumina membranes. *J. Colloids Interface Sci.* **2012**, *376*, 40–46. [CrossRef] [PubMed]
15. Prida, V.M.; Vega, V.; García, J.; Iglesias, L.; Hernando, B.; Minguez-Bacho, I. Electrochemical Methods for Template-Assisted Synthesis of Nanostructured Materials. In *Magnetic Nano- and Microwires*; Vázquez, M., Ed.; Woodhead Publishing: Cambridge, UK, 2015; pp. 1–39, ISBN 9780081001646.
16. Meng, X.; Norouzi Banis, M.; Geng, D.; Li, X.; Zhang, Y.; Li, R.; Abou-Rachid, H.; Sun, X. Controllable atomic layer deposition of one-dimensional nanotubular TiO_2. *Appl. Surf. Sci.* **2013**, *266*, 132–140. [CrossRef]
17. Moulder, J.F.; Stickle, W.F.; Sobol, P.E.; Bomben, K.D. *Handbook of X-ray Photoelectron Spectroscopy*; Chastain, J., Ed.; Perkin-Elmer Corporation: Minneapolis, MN, USA, 1992.
18. Schneider, C.A.; Rasband, W.S.; Eliceiri, K.W. NIH Image to ImageJ: 25 years of image analysis. *Nat. Methods* **2012**, *9*, 671–675. [CrossRef] [PubMed]
19. Romero, V.; Vázquez, M.I.; Benavente, J. Study of ionic and diffusive transport through a regenerated cellulose nanoporous membrane. *J. Membr. Sci.* **2013**, *433*, 152–159. [CrossRef]
20. Nielsch, K.; Choi, J.; Schwirn, K.; Wehrspohn, R.B.; Gösele, U. Self-ordering regimes of porous alumina: The 10% porosity rule. *Nano Lett.* **2002**, *2*, 677–680. [CrossRef]
21. Weirich, T.E.; Winterer, M.; Seifried, S.; Fuess, H.; Hahn, H. Rietveld analysis of electron powder diffraction data from nanocrystalline anatase TiO_2. *Ultramicroscopy* **2000**, *81*, 263–270. [CrossRef]
22. Ariza, M.J.; Benavente, J.; Rodríguez-Castellón, E. The Capability of X-ray Photoelectron Spectroscopy in the Characterization of Membranes: Correlation between Surface Chemical and Transport Properties in Polymeric Membranes. In *Handbook of Membrane Research: Properties, Performance and Applications*; Nova Science Publishers, Inc.: New York, NY, USA, 2009; Chapter 7; pp. 257–290. ISBN 978-1-60741-638-8.
23. Vega, V.; Gelde, L.; González, A.S.; Prida, V.M.; Hernando, B.; Benavente, J. Diffusive transport through surface functionalized nanoporous alumina membranes by atomic layer deposition of metal oxides. *J. Ind. Eng. Chem.* **2017**, *52*, 66–72. [CrossRef]
24. Thompson, D.W.; Snyder, P.G.; Castro, L.; Yan, L. Optical characterization of porous alumina from vacuum ultraviolet to midinfrared. *J. App. Phys.* **2005**, *97*, 113511–113519. [CrossRef]

25. Gâlca, A.C.; Kooij, E.S.; Wormeester, H.; Salm, C.; Lecca, V.; Rector, J.H.; Poelsema, B. Structural and optical characterization of porous anodic aluminium oxide. *J. Appl. Phys.* **2003**, *94*, 4296–4305. [CrossRef]
26. Ogielo, W.; Wormeester, H.; Wessling, M.; Benes, N.E. Spectroscopic ellipsometry analysis of a thin film composite membrane consisting of polysulphone on a porous α-alumina support. *ACS Appl. Mater. Interfaces* **2012**, *4*, 935–943. [CrossRef] [PubMed]
27. Fujiwara, H. *Spectroscopic Ellipsometry Principles and Applications*; John Wiley & Sons: Chischester, UK, 2007; ISBN 9780470016084.
28. Jeon, G.; Yang, S.Y.; Kim, J.K. Functional nanoporous membranes for drug delivery. *J. Mater. Chem.* **2012**, *22*, 14814–14834. [CrossRef]
29. Kuo, T.-C.; Sloan, L.A.; Sweedler, J.V.; Bohn, P.W. Manipulating Molecular Transport through Nanoporous Membranes by Control of Electrokinetic Flow: Effect of Surface Charge Density and Debye Length. *Langmuir* **2001**, *17*, 6298–6303. [CrossRef]
30. Robinson, R.A.; Stokes, R.H. *Electrolyte Solutions*, 2nd ed.; Dover Publications: New York, NY, USA, 2002; ISBN 0486422259.
31. Sollner, K. The Electrochemistry of Porous Membranes, with Particular Reference to Ion Exchange Membranes and Their Use in Model Studies of Biophysical Interest. *J. Macromol. Sci. Pure Appl. Chem.* **1969**, *3*, 1–86. [CrossRef]
32. Meyer, K.H.; Sievers, J.F. La perméabilité des membranes I. Théorie de la perméabilité ionique. *Helv. Chim. Acta* **1936**, *19*, 649–664. [CrossRef]
33. Teorell, T. Transport phenomena in membranes eighth Spiers Memorial Lecture. *Discuss. Faraday Soc.* **1956**, *21*, 9–26. [CrossRef]
34. Lakshminarayanaiah, N. *Transport Phenomena in Membranes*; Academic Press Inc.: New York, NY, USA, 1970; ISBN1 10: 0124342507, ISBN2 13: 9780124342507.
35. Romero, V.; Vega, V.; García, J.; Prida, V.M.; Hernando, B.; Benavente, J. Effect of porosity and concentration polarization on electrolyte diffusive transport parameters through ceramic membranes with similar nanopore size. *Nanomaterials* **2014**, *4*, 700–711. [CrossRef] [PubMed]
36. Romero, V.; Vázquez, M.I.; Cañete, S.; Vega, V.; García, J.; Prida, V.M.; Hernando, B.; Benavente, J. Frictional and Electrical Effects Involved in the Diffusive Transport through a Nanoporous Alumina Membrane. *J. Phys. Chem. C* **2013**, *117*, 25513–25518. [CrossRef]